European Polymer Journal 254 (2026) 114848

Contents lists available at ScienceDirect

European Polymer Journal

journal homepage: www.elsevier.com/locate/europolj

POSS-containing CO_2-derived diblock copolymer templating for thermally robust mesoporous phenolic resins via competitive hydrogen bonding and reaction-induced microphase separation

Yen-Min Lo [a], Yen-Ling Kuan [a], Yang-Chin Kao [a], Junko Aimi [b], Chih-Feng Huang [c,f], U-Ser Jeng [d], Shiao-Wei Kuo [a,e,*]

[a] Department of Materials and Optoelectronic Science, Center for Functional Polymers and Supramolecular Materials, National Sun Yat-Sen University, Kaohsiung 80424, Taiwan
[b] Research Center for Macromolecules and Biomaterials, National Institute for Materials Science, 1-2-1 Sengen, Tsukuba, Ibaraki 305-0047, Japan
[c] Department of Chemical Engineering, i-Center for Advanced Science and Technology (iCAST), National Chung Hsing University, Taichung 402-27, Taiwan
[d] National Synchrotron Radiation Research Center, Hsinchu 30076, Taiwan
[e] Department of Medicinal and Applied Chemistry, Kaohsiung Medical University, Kaohsiung 807, Taiwan
[f] Graduate Program in Semiconductor and Green Technology, Academy of Circular Economy, National Chung Hsing University, Nantou City, Nantou County 540216, Taiwan.

A B S T R A C T

We proposed the POSS-containing diblock copolymer from CO_2-derived polycarbonates templating strategy to prepare mesoporous phenolic resins. Two PEO-*b*-PCHCPOSS diblock copolymers were synthesized by using PEO as a macroinitiator with cyclohexene oxide (CHO), epoxycyclohexyl isobutyl POSS (CHOPOSS), and CO_2 based on LZn_2 (OAc) $_2$ as the catalyst via ring-opening copolymerization (ROCOP). The formation of linear carbonate backbones with the incorporation of POSS cages of these diblock copolymers were confirmed by FTIR, ^{1}H, ^{13}C, ^{29}Si, and DOSY NMR, and GPC analyses. Binary blends of PEO-*b*-PCHCPOSS diblock copolymers with phenolic resin exhibit two composition-dependent glass transition temperatures (T_{gs}), indicating the microphase separation governed by competitive hydrogen bonding between OH units of phenolic resin with ether groups of PEO, carbonate C=O units of PCHC, and siloxane units of POSS cage. Small-angle X-ray scattering (SAXS) patterns reveal that the reaction induced microphase separation (RIMPS) to generate short-range-order self-assembled nanostructures of phenolic/PEO-*b*-PCHCPOSS blends upon thermal curing at 150 °C. Subsequent pyrolysis at 350 °C could remove the block copolymer template and yields mesoporous phenolic frameworks with tunable pore sizes, corroborated by TEM images and N_2 adsorption–desorption isotherms analyses. Notably, the POSS moieties, covalently anchored to the PCHC segments, are preferentially retained at the pore walls after template removal, leading to inorganic cage-enriched pore surfaces that enhance structural stability and inhibit pore collapse during thermal processing. In addition, increasing POSS loading from 2 to 5 wt% preserves the mesoscale length but reduces structural coherence, consistent with packing frustration imposed by rigid cages and phenolic/POSS hydrogen bonding competition. This work establishes a CO_2-derived diblock copolymer/POSS hybrid templating platform for thermally robust mesoporous phenolic materials with controllable self-assembled nanostructure.

1. Introduction

Mesoporous phenolic materials have attracted much interest due to their high thermal stability, chemical resistance, and tunable pore architectures, which make them promising candidates for applications in catalysis, energy storage, adsorption, and separation technologies [1–7]. Among these various synthetic strategies, the self-assembled behavior of diblock copolymers as soft-templating approaches are particularly interesting, as they allow precise control pore size and nanoscale ordering through molecular design by controlling degree of polymerization (N), Flory-Huggins interaction parameter (χ), and volume fraction (f) [8–12]. However, achieving the well-defined nanostructures in phenolic resin remains challenging owing to the complex interplay between self-assembly behavior, competitive hydrogen bonding, and thermally induced crosslinking reactions.

Reaction-induced microphase separation (RIMPS) have emerged as a powerful concept to address these challenges. In such systems, a non– or weakly segregated diblock copolymer with phenolic resin can evolve into the short-range or long-range ordered nanostructure during thermal polymerization, as chemical reactions progressively increase segregation strength (χN value) and immobilize the evolving morphology [13–15]. Phenolic resin is particularly well suited to this approach,

* Corresponding author at: Department of Materials and Optoelectronic Science, Center for Functional Polymers and Supramolecular Materials, National Sun Yat-Sen University, Kaohsiung 80424, Taiwan.
E-mail address: kuosw@faculty.nsysu.edu.tw (S.-W. Kuo).

https://doi.org/10.1016/j.eurpolymj.2026.114848
Received 15 March 2026; Received in revised form 30 April 2026; Accepted 23 May 2026
Available online 24 May 2026

during thermal polymerization could introduce extensive hydrogen bonding and crosslinking, which can amplify compositional contrast and stabilize transient self-assembled nanostructures [16–18]. However, the structural regularity and thermal robustness of phenolic-derived mesoporous frameworks are often limited by framework shrinkage, pore collapse, or insufficient control over the template–matrix interactions. In general, the poly(ethylene oxide)-based diblock copolymers including PEO-*b*-PCL, PEO-*b*-PS, PEO-*b*-PMMA, PEO-*b*-PBLG, and PEO-*b*-PLA have been widely used as the templates to fabricate the mesoporous materials [9,19–22].

In addition, the carbon dioxide (CO_2)-derived block polymers has become an important research direction in sustainable polymer chemistry [23–25]. Ring-opening copolymerization (ROCOP) of epoxy derivatives with CO_2 provides an efficient route to aliphatic polycarbonates with well-defined architectures, inherent hydrogen-bonding capability, and adjustable polarity [26–28]. These CO_2-derived polycarbonates have recently been explored as soft templates for nanostructured materials; for example, we have synthesized the poly (ethylene oxide-*b*-cyclohexene carbonate) (PEO-*b*-PCHC), as a template to fabricate mesoporous phenolic resin by using thermal polymerization at 150 °C and subsequent pyrolysis at 350 °C [29]. However, their relatively lower segregation strength (χN value) and limited thermal stability would restrict their effectiveness in directing ordered nanostructures, particularly in phenolic resins that undergo harsh thermal processing.

Polyhedral oligomeric silsesquioxane (POSS) cage represents an attractive strategy to address these limitations, which combines the rigid inorganic Si-O-Si cage structure with tunable organic substituents, offering improved thermal stability, and strong interfacial affinity toward phenolic resin [30–34]. Incorporating inorganic POSS cage into diblock copolymers have been observe to modify chain packing, and improve the Flory-Huggins interaction parameter (χ) value and thermal robustness of self-assembled nanostructures [16,35–38]. In despite these advantages, the role of covalently tethered POSS cages in CO_2-derived block copolymers as the templates to fabricate mesoporous phenolic resin via reaction induced microphase separation, remains insufficiently understood.

Herein, we report the POSS-containing CO_2-derived diblock copolymer templating strategy to fabricate mesoporous phenolic resins with tunable self-assembled nanostrucutre. PEO-*b*-PCHCPOSS diblock copolymers were synthesized via ROCOP of cyclohexene oxide, epoxy-functionalized isobutyl POSS, and CO_2 using PEO as a macroinitiator

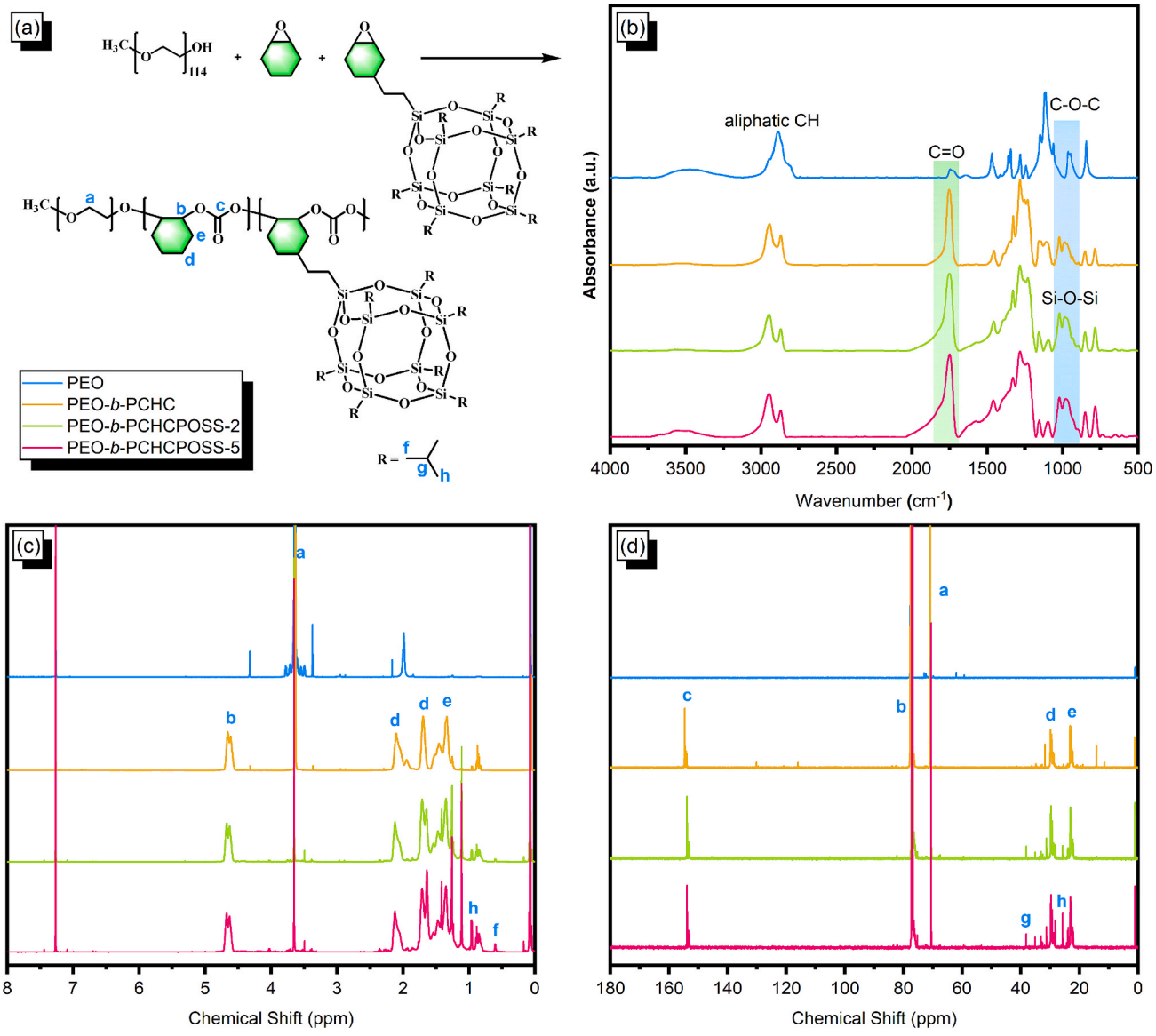

Fig. 1. (a) The synthesis of PEO-*b*-PCHCPOSS diblock copolymers and their (b) FTIR, (c) ^{1}H and (d) ^{13}C NMR analyses.

(Fig. 1(a)). The covalent incorporation of intact POSS cages into the PCHC block segment enhances thermal stability while introducing controlled packing constraints. When blended with phenolic resin, these diblock copolymers form microphase separation behavior governed by competitive hydrogen bonding interaction strength among phenolic OH groups with PEO C-O-C units, PCHC carbonate C=O units, and POSS siloxane cages. Thermal curing induces reaction-induced microphase separation, while subsequent pyrolysis removes the polymer template to yield mesoporous phenolic frameworks. By systematically varying the phenolic content and POSS loading (2 and 5 wt%), we elucidate the hydrogen-bond competition, inorganic cage effects, and thermal processing collectively dictate pore size, surface area, and structural coherence. SAXS, TEM, and N_2 sorption analyses reveal that moderate POSS loading promotes uniform mesoporous architectures, whereas higher POSS contents introduce packing frustration and reduce long-range correlation while preserving the nanoscale length scale and also leads to inorganic cage-enriched pore surfaces that enhance structural stability and inhibit pore collapse during thermal processing. This work provides new insights into the design of CO_2-derived polymer/POSS hybrid templates and establishes a versatile platform for engineering thermally robust mesoporous phenolic materials through controlled reaction-induced self-assembled behavior.

2. Experimental section

2.1. Materials

Sodium hydroxide (97%), calcium hydride (CaH_2), cyclohexene oxide (CHO), and hydrochloric acid (HCl) were sourced from SHOWA. Poly(ethylene oxide) methyl ether (PEO, M_n = 5000 Da) was procured from Sigma Aldrich. Dichloromethane (DCM), methanol (MeOH), tetrahydrofuran (THF), and *n*-hexane were purchased from Thermo Fisher Scientific. High purity of CO_2 (> 99.999%) was supplied from Hsin E-Li Gas Industrial Co., Ltd. Epoxycyclohexyl isobutyl POSS (CHOPOSS) was obtained from Kingpak Technology Inc., without further purification. The catalyst of $LZn_2(OAc)_2$ was synthesized following our previous reported procedure [39–43] and the phenolic resin (resol-type) (Scheme S1) was also widely proposed by our previous literatures [16,17].

2.2. Synthesis of PEO-b-PCHCPOSS diblock copolymers through ROCOP

Two PEO-*b*-PCHCPOSS diblock copolymers were synthesized through the ring-opening copolymerization (ROCOP) from CHO, CHOPOSS, and CO_2, using PEO as the macroinitiator. Before polymerization, CHO was dried over calcium hydride (CaH_2) and purified by vacuum distillation, while CHOPOSS was dehydrated through heat-assisted vacuum distillation. The purified CHO and CHOPOSS monomers were then premixed to ensure homogeneity before introduction into the reactor. The catalyst $LZn_2(OAc)_2$ was charged into a stainless-steel autoclave equipped with a magnetic stir bar and connected to a vacuum line. The catalyst (0.023 g, 0.07 mmol) and PEO (1.0 g, 0.002 mmol) were dried under vacuum at 50 °C for 10 h. After purging with CO_2, CHO (7.1 mL, 0.07 mol) and 2 or 5 wt% CHOPOSS was added to the reactor. The copolymerization was carried out at 80 °C under a constant CO_2 pressure of 440 psi for 20 h. Upon completion, the autoclave was cooled to room temperature, and the residual CO_2 was carefully released. The crude product was dissolved in dichloromethane (DCM) and washed repeatedly with 5% aqueous hydrochloric acid until the aqueous phase became clear. The organic layer was concentrated and precipitated several times in an ice bath, followed by washing with hexane to remove residual impurities. The resulting solid was dried under vacuum at 30 °C to yield PEO-*b*-PCHCPOSS as a white powder [41]. FTIR (KBr, cm^{-1}): 2850–2960 (aliphatic CH), 1751 (C=O), 1100 (Si–O–Si and C-O-C). 1H NMR (500 MHz, $CDCl_3$, δ, ppm): 4.66 (Cy**C**HOCO$_2$), 3.64 (C**H**$_2$C**H**$_2$O), 2.21–1.25 (CyC**H**$_2$), 1.85 (Si–CH$_2$–C**H**–(CH$_3$)$_2$), 0.96 (Si–CH$_2$–CH–(C**H**$_3$)$_2$), 0.60 (Si–C**H**$_2$–CH–(CH$_3$)$_2$). ^{13}C NMR (125 MHz, $CDCl_3$, δ, ppm): 154.5 (C=O), 74.0 (C-O from PCHC), 70.9 (C–O from PEO), 32.6 (Si–CH$_2$–**C**H–(CH$_3$)$_2$), 22.7–29.8 (CyCH$_2$).

2.3. Preparation of Phenolic/PEO-b-PCHCPOSS binary blend

Blends containing various weight ratios of phenolic resin and the PEO-*b*-PCHCPOSS diblock copolymers were prepared by dissolving both components thoroughly in THF under continuous stirring to ensure complete miscibility and homogeneity. The resulting clear solutions were then carefully cast into aluminum pans. To achieve uniform thin films, the solvent was allowed to evaporate gradually at ambient temperature in an open environment, which helped to minimize the occurrence of macroscopic phase separation. After most of the THF had evaporated, the films were further dried under vacuum at 30 °C for 24 h. This drying step ensured the complete removal of residual solvent and provided stabilization of the self-assembled nanostructures that had developed during the solvent evaporation process. The phenolic/PEO-*b*-PCHCPOSS blends were prepared in various weight ratios, specifically 100/0, 70/30, 60/40, 50/50, 40/60, 30/70, and 0/100 (w/w).

2.4. The preparation of thermally induced mesoporous phenolic resins

The dried blend films were subsequently subjected to thermal curing following a well-controlled heating protocol. Specifically, the samples were heated from room temperature to 150 °C at a slow heating rate of 1 °C min^{-1}, followed by an isothermal treatment at this temperature for 24 h to promote thorough cross-linking of the phenolic resin. After curing, the cross-linked hybrid materials were further pyrolyzed under similar heating conditions. During this step, the temperature was raised to 350 °C at the same slow heating rate of 1 °C min^{-1} and maintained for an additional 24 h. This extended thermal treatment not only ensured the efficient removal of the PEO-*b*-PCHCPOSS copolymer template but also facilitated the development of ordered mesoporous phenolic resin framework.

3. Results and discussion

3.1. The synthesis of PEO-b-PCHCPOSS diblock copolymers

Fig. 1(a) displays the schematic illustration of the ring-opening copolymerization (ROCOP) of CHO, CHOPOSS, and CO_2 initiated by PEO-OH, yielding PEO-*b*-PCHCPOSS diblock copolymers with tunable POSS incorporation. The chemical structure highlights the PEO block segment the PCHC repeating units, and the covalently tethered POSS cages. The FTIR spectra of PEO, PEO-*b*-PCHC and PEO-*b*-PCHCPOSS (2 and 5 wt% POSS) diblock copolymers (denoted PEO-*b*-PCHCPOSS-2 and PEO-*b*-PCHCPOSS-5) as shown in Fig. 1(b) demonstrates the evolution of characteristic vibrational absorptions. A distinct and intense absorption band attributed to the carbonate C=O stretching vibration appears at 1750 cm^{-1}, accompanied by the C-O-C and Si–O–Si stretching bands within the 1100 cm^{-1} range. These spectral characteristics confirm the successful preparation of the PEO-*b*-PCHCPOSS diblock copolymer and indicate the formation of a linear polycarbonate backbone rather than a cyclic carbonate configuration [44,45]. Fig. 1(c) shows ^{1}H NMR spectra of each polymer segment. The methine proton corresponding to the cyclohexyl CH unit on the PCHC main chain at 4.66 ppm (*a*) and the CH_2 unit of the PEO block resonates at 3.64 ppm (*b*), confirming the formation of diblock copolymer. Cyclohexyl methylene protons from the PCHC segment (*d* and *e*, 1.33–2.11 ppm) and the isobutyl protons of POSS cage at 0.6 ppm (Si-CH_2), 0.96 ppm (CH_3), and 1.85 (CH) systematically increase in intensity with POSS incorporation. Using the integral areas of PEO CH_2 signal (3.64 ppm), CH unit of the PCHC block (4.66 ppm) and the CH unit of POSS cage (0.60 ppm), the molecular weight of each block in the resulting copolymers were calculated, as summarized in Table 1. Fig. 1(d) displays ^{13}C NMR further confirms the

Table 1
Physical properties of PEO-*b*-PCHC and PEO-*b*-PCHCPOSS diblock copolymers used in this study.

Copolymers[a]	%PC	POSS (wt%)	Conv. (CHO)	TON	TOF (h^{-1})	M_n (Da)	$Đ^b$	T_g (°C)	T_{d10} (°C)
PEO-*b*-PCHC	>99	–	76.5	26	1.3	55,070	1.43	80	314
PEO-*b*-PCHCPOSS-2	>99	1.04	91.5	4.1	0.2	59,800	1.62	75	317
PEO-*b*-PCHCPOSS-5	>99	2.57	90.9	9.9	0.5	60,300	1.58	68	310

[a] All [M]:[I]:[Catalyst] = 1000:2.85:1, [b]determined by GPC analyses.

diblock copolymers. The carbonate carbon signal (*c*, 154.57 ppm) evidences the PCHC formation, while PEO carbons (*b*, 70.86 ppm) remain unchanged. The backbone cyclohexyl CH carbon resonance of PCHC is observed at 77.10 ppm, while the corresponding side-chain carbons appear at 23.16 and 29.82 ppm. The Si–$CH_2CH(CH_3)_2$ carbon from the POSS cage is detected at 32.4 ppm.

To evaluate the molecular characteristics of the diblock copolymers, the relative molecular weights were also measured through gel permeation chromatography (GPC) analyses as displayed in Fig. 2(a). Since the PEO macroinitiator a principal low-molar-mass peak at longer elution time together with a minor high-molar-mass shoulder at shorter elution time, corresponding to small amount of aggregated species. After chain extension via ROCOP to form PEO-*b*-PCHC, the main elution peak shifts to shorter elution time, consistent with an increase in molar mass. A further shift of the peaks for PEO-*b*-PCHCPOSS-2 and PEO-*b*-PCHCPOSS-5 to even shorter elution times confirms successful incorporation of CHOPOSS into the block copolymer backbone while maintaining a reasonably narrow molecular weight distribution, where the number-average molecular weight (M_n) and polydispersity index (PDI) of PEO-*b*-PCHCPOSS with 2 wt% POSS were 59,800 g/mol and 1.62, whereas those of PEO-*b*-PCHCPOSS with 5 wt% POSS were 60,300 g/mol and a PDI of 1.58. To verify that POSS is covalently tethered to the diblock copolymer rather than present as a separate species, DOSY NMR experiments were performed as shown in Fig. 2(b) and (c). For both the 2 and 5 wt% POSS samples, all resonances—those assigned to the PEO segment, the PCHC backbone, and the isobutyl groups of the POSS cages—share essentially the same diffusion coefficient. The absence of signals with distinct diffusion behavior demonstrates that free CHOPOSS or detached POSS-containing fragments are negligible, and that the POSS cages are incorporated into a single diffusing macromolecular entity.

The silicon environment in the PEO-*b*-PCHCPOSS diblock copolymers were further confirmed by ^{29}Si NMR spectroscopy (Fig. 2(d)). A dominant resonance appears at approximately − 70 ppm, characteristic of fully condensed T_8 silsesquioxane cages ($RSiO_{1.5}$) and confirming that the cage integrity is preserved during the ROCOP process. These results corroborate the successful introduction of intact CHOPOSS units along the PCHC block. The thermal analyses were characterized by DSC as displayed in Fig. 2(e). Pure PEO exhibits the pronounced melting endotherm near 60 °C, characteristic of its semicrystalline nature. After

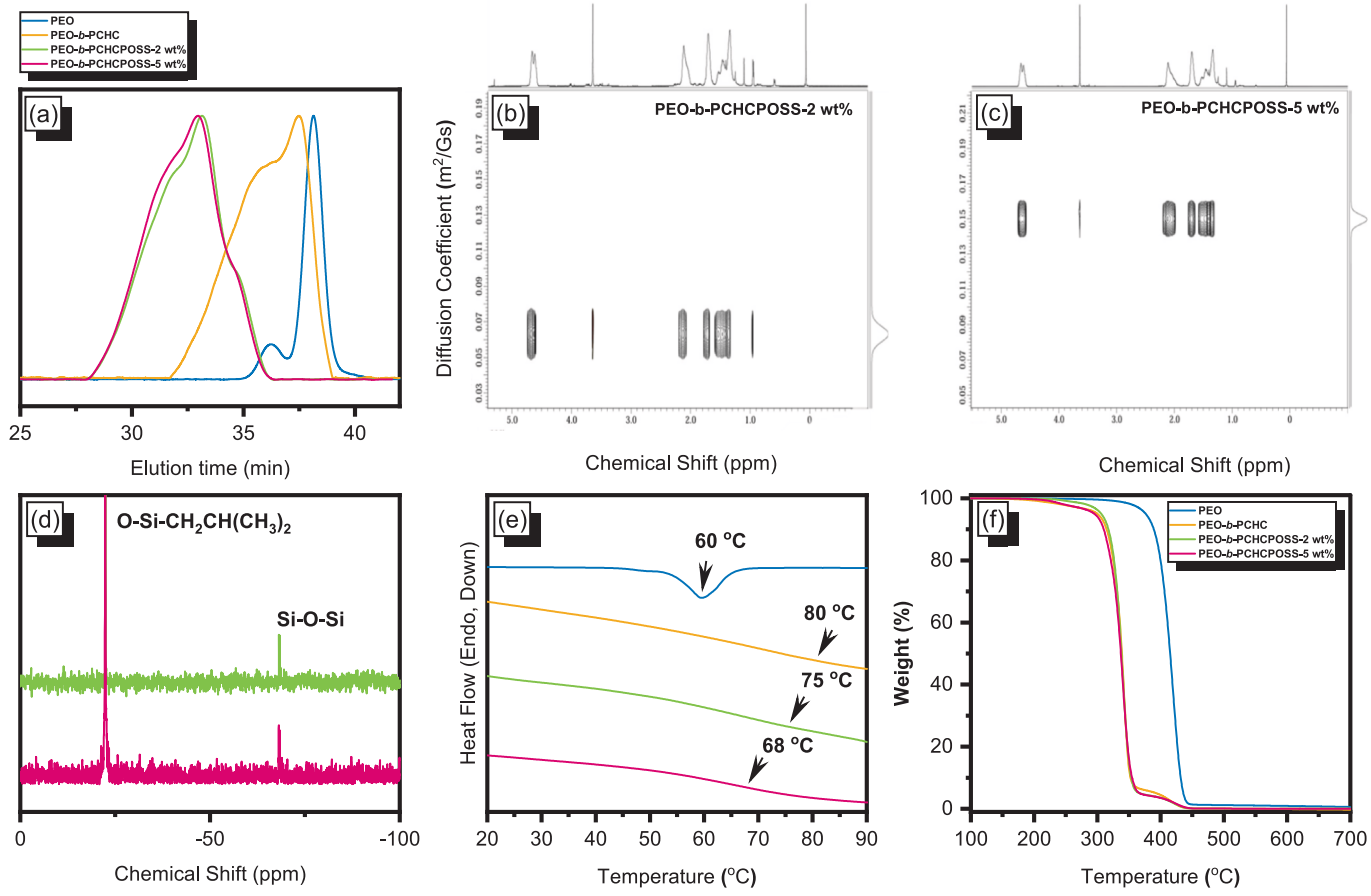

Fig. 2. (a) GPC analyses, (b, c) DOSY spectra of PEO-*b*-PCHCPOSS-2 and PEO-*b*-PCHCPOSS-5, (d) ^{29}Si NMR, (e) DSC analyses and (f) TGA analyses of PEO, PEO-*b*-PCHC, and PEO-*b*-PCHCPOSS diblock copolymers.

ROCOP to form PEO-*b*-PCHC diblock copolymer, the melting endotherm is markedly reduced, indicating a substantial suppression of PEO crystallinity due to the presence of the rigid carbonate block and the resulting disorder structure since PEO/PCHC binary blends, the melting behavior was still observed in Fig. S1. For the PEO-*b*-PCHCPOSS diblock copolymers, the endothermic peak is also diminished, and the glass transition temperature from 80 °C of PEO-*b*-PCHC shifted to 75 °C and 67 °C for 2 wt% and 5 wt% POSS compositions, respectively. Since the bulky POSS case as the side chain might increase the free volume and induce the dilution effect, which also decrease the intramolecular hydrogen bonding or dipole–dipole interactions and of PCHC segment as discussed in our previous study.[27,38] The thermal stability of these polymers was also evaluated by TGA under nitrogen as displayed in Fig. 2(f). Neat PEO shows a single, rapid weight-loss event at higher temperature, whereas PEO-*b*-PCHC exhibits a noticeable shift of the degradation onset to lower temperature, reflecting the decreasing the thermal stability of the carbonate-containing block. Incorporation of POSS could improve the high-temperature behavior: both PEO-*b*-PCHCPOSS diblock copolymers display slightly higher decomposition temperatures and residual weights at 800 °C, attributable to the thermally robust silsesquioxane cages. All physical properties of these diblock copolymers used in this study were summarized in Table 1.

3.2. The preparation of Phenolic/PEO-b-PCHCPOSS binary blends

Fig. 3(a) and 3(b) display DSC thermal analyses of phenolic/PEO-*b*-PCHCPOSS blends containing (a) 2 wt% and (b) 5 wt% POSS, which all reveal two distinct T_g values across all blend compositions. Pure phenolic resin exhibits a T_g value near −53 °C, while the diblock copolymers show progressively higher T_g value depending on their composition and POSS content as shown in Fig. 2(e). The lower-temperature T_g value is associated with the rich phenolic/PEO domain phase, whereas the higher-temperature T_g value corresponds to the rich phenolic/PCHCPOSS domain phase. The presence of two T_g values demonstrates that the blends are not fully miscible and may form partially miscible or microphase-separated structures. The composition dependence of T_g values for these three diblock copolymers (PEO-*b*-PCHC, PEO-*b*-PCHCPOSS-2, and PEO-*b*-PCHCPOSS-5) and the T_g

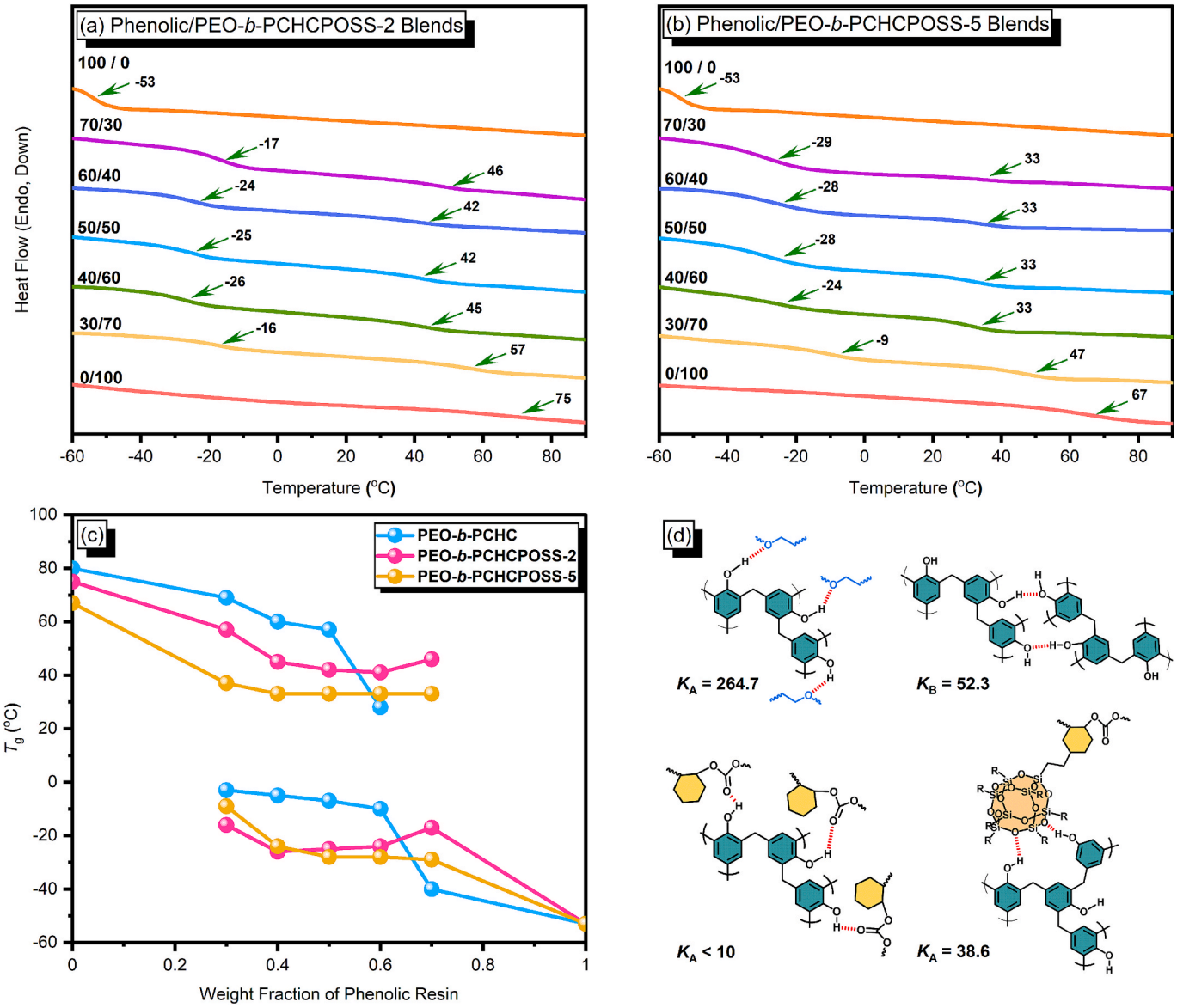

Fig. 3. DSC analyses of (a) phenolic/PEO-*b*-PCHCPOSS-2 blends and (b) phenolic/PEO-*b*-PCHCPOSS-5 blends, (c) T_g composition behavior of phenolic/PEO-*b*-PCHCPOSS blends, and (d) the scheme of hydrogen bonding interaction of inter-association and self-association equilibrium constant in phenolic/PEO blend (K_A = 264.7), pure phenolic (K_B = 52.3), phenolic/POSS blend (K_A = 38.6), and phenolic/PCHC blend (K_A < 10).

composition plots confirm the existence of two distinct thermal transitions for all blends as displayed in Fig. 3(c).

TGA curves of representative phenolic/PEO-*b*-PCHCPOSS-5 blends have been added to evaluate their thermal stability and decomposition behavior, as shown in Fig. S2. Compared to the neat copolymer, the blends exhibit significantly higher thermal residue, which increases with phenolic content. This indicates the formation of a thermally stable carbonaceous network derived from phenolic resin. In addition, the gradual weight loss at elevated temperatures suggests the coexistence of polymer decomposition and carbonization processes. The presence of POSS further contributes to the formation of inorganic Si–O residues, which enhances the thermal stability of the system. These results support that, although partial decomposition of organic components occurs below 300 °C, the overall system evolves into a stable hybrid (carbon/silica-like) framework, which is essential for maintaining the mesostructure after template removal.

Fig. 4 shows the FTIR spectra of the phenolic/PEO-*b*-PCHCPOSS binary blends, focusing on the OH stretching region (3800–3200 cm^{-1}) and the carbonyl (C=O) stretching region (1780–1700 cm^{-1}) at two POSS loadings (2 wt% and 5 wt%). The systematic peak shifts observed for both functional groups provide direct evidence of hydrogen-bonding interactions between phenolic hydroxyl groups and the ether groups of PEO, carbonate carbonyl groups of PCHC and siloxane group of POSS cage in the block copolymer matrix. For both 2 wt% (a) and 5 wt% (c) POSS-containing samples, the broad OH stretching band progressively shifts from higher wavenumber (3520–3480 cm^{-1}) toward lower wavenumber (3400–3350 cm^{-1}) as the phenolic content increases from 30/70 to 70/30, indicating the hydrogen bonding environments become more heterogeneous.

The carbonate C=O stretching region of PCHCPOSS exhibits two characteristic peaks where the absorption peak at 1763 cm^{-1} due to the free C=O units and 1738 cm^{-1} corresponding to the intramolecular hydrogen bonding of C=O···H-C unit in six-membered ring as shown in Fig. 4(b) and (d), confirming that the PCHC backbone inherently contains both free and hydrogen bonded C=O species. Carbonate C=O stretching peak of PCHCPOSS gradually shifts to lower wavenumbers upon increasing phenolic contents. In addition, a peak appears for the C=O units at 1720 cm^{-1}, suggesting the formation of intermolecular hydrogen bonding interaction between phenolic OH units and the C=O units of PCHCHPOSS units. To quantify these different C=O units of each peaks, Fig. 5(a) and (c) exhibit the curve fitting results of the carbonate C=O groups of phenolic/PEO-*b*-PCHCPOSS-2 and phenolic/PEO-*b*-PCHCPOSS-5 binary blends with various compositions, which were summarized in Fig. 5(b) and (d). Increasing the phenolic compositions, free and intramolecular hydrogen bonded C=O units were both decreased and the intermolecular hydrogen bonded C=O units with phenolic OH units were slightly increased and the POSS loading with 5 wt% is generally lower than 2 wt% since the distinct screening effect

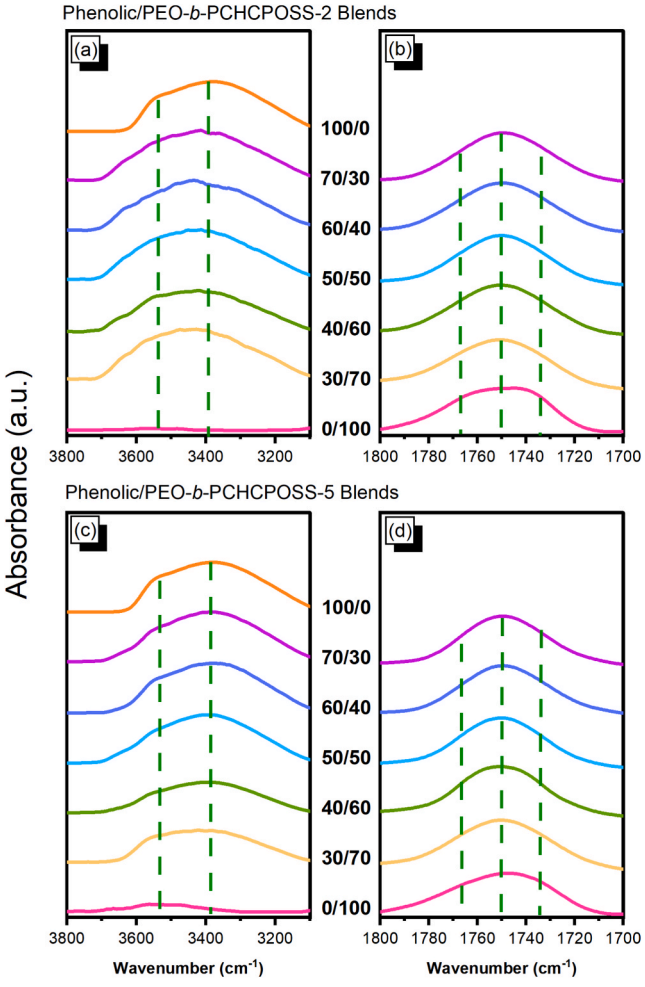

Fig. 4. FTIR spectra of (a) OH and (b) C=O regions of phenolic/PEO-*b*-PCHCPOSS-2 blends, (c) OH and (d) C=O regions phenolic/PEO-*b*-PCHCPOSS-5 blends recorded at room temperature.

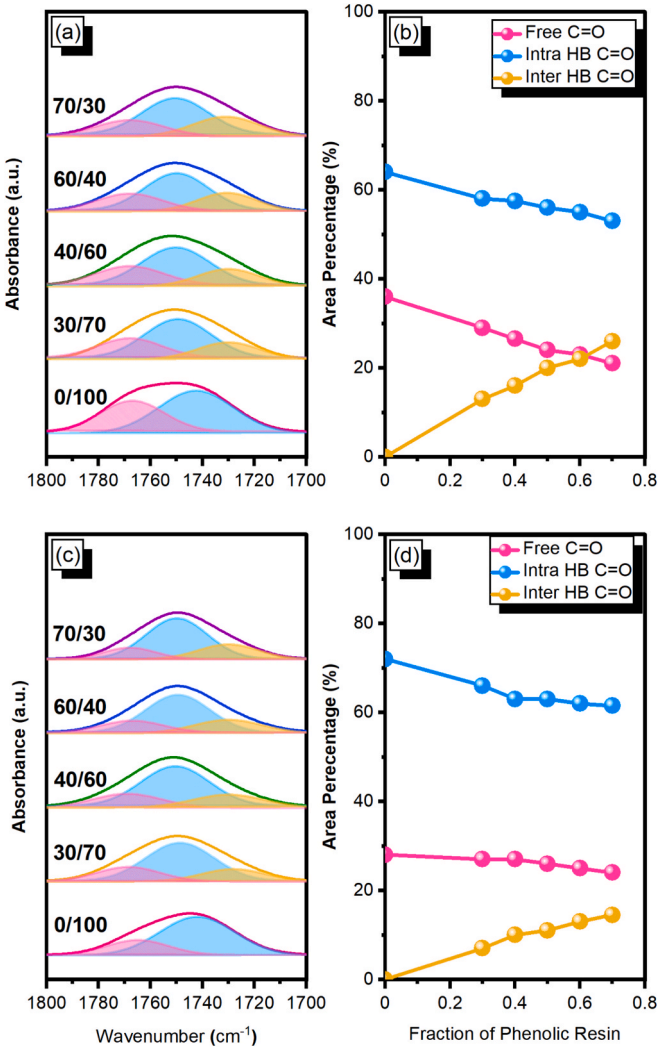

Fig. 5. FTIR spectra curve fitting results of C=O region of (a) phenolic/PEO-*b*-PCHCPOSS-2 blends and (b) their corresponding area percentage, (c) phenolic/PEO-b-PCHCPOSS-5 blends and their corresponding area percentage of free, intra-HB and inter-HB C=O units.

from the POSS cage structure and phenolic OH units also prefer to interact with siloxane group of POSS cage ($K_A = 38.6$) rather than PCHC C=O units ($K_A < 10$). Briefly, K_A and K_B are equilibrium constants defined based on the Painter–Coleman association model [46,47]. K_A represents intermolecular hydrogen bonding between different functional groups, while K_B corresponds to self-association (OH···OH) within the phenolic matrix. All possible hydrogen bonding interactions in phenolic/PEO-*b*-PCHCPOSS binary blends were summarized in Fig. 3(d) [29,30,46]. We could understand that the hydrogen bonding strength of phenolic OH units in phenolic/PEO-*b*-PCHCPOSS blends by the following order: phenolic/PEO ($K_A = 286$) > phenolic/phenolic ($K_B = 52.3$) > phenolic/POSS ($K_A = 38.6$) > phenolic/PCHC ($K_A < 10$).

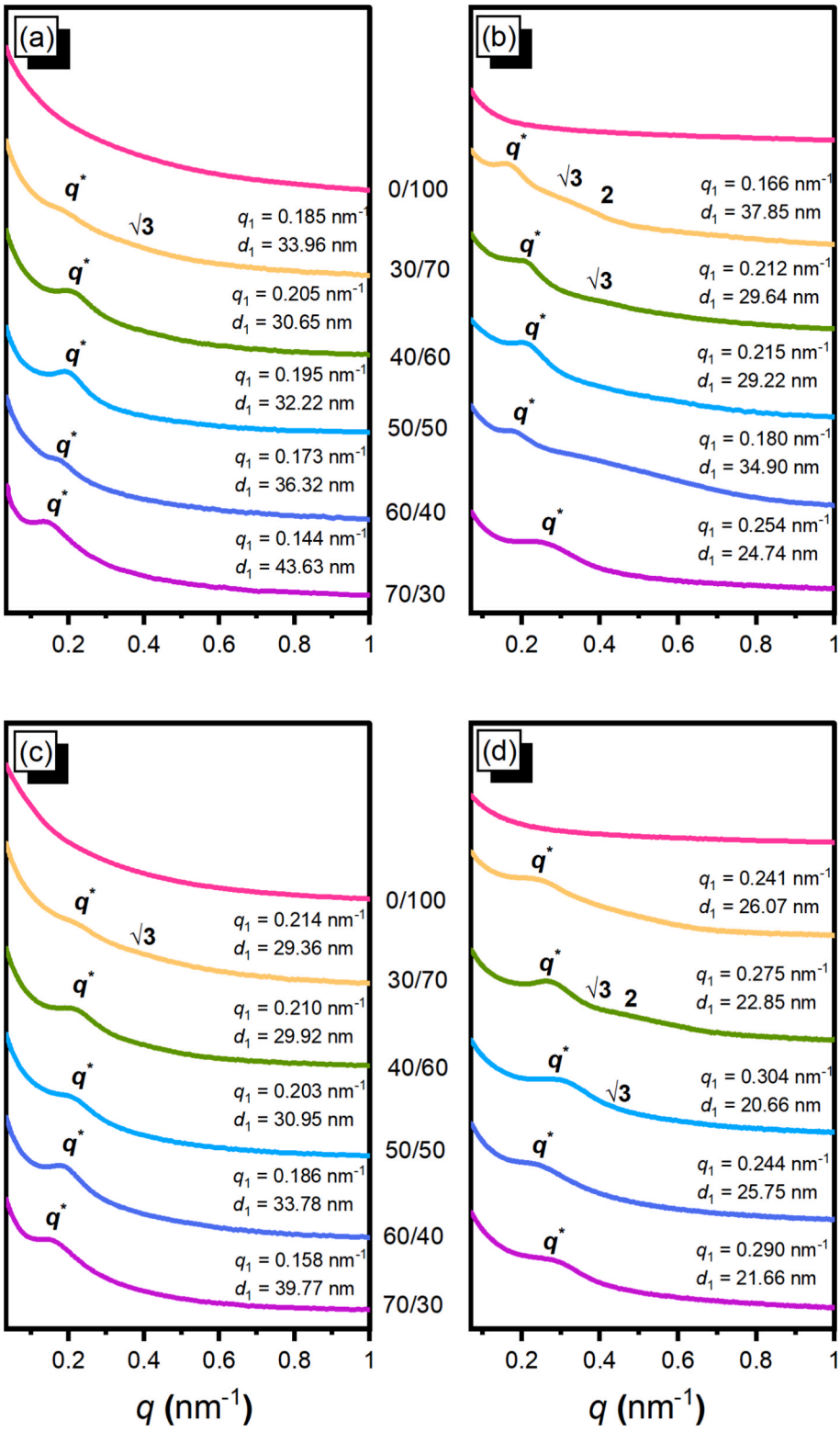

Fig. 6. SAXS patterns of phenolic/PEO-*b*-PCHCPOSS blends before and after thermal curing at 150 °C: (a) PCHCPOSS-2 before curing, (b) PCHCPOSS-2 after thermal curing, (c) PCHCPOSS-5 before curing, and (d) PCHCPOSS-5 after thermal curing.

Consequently, the FTIR analysis provides a coherent molecular-level picture indicating that hydrogen bonding competition, especially between phenolic/PEO and phenolic/POSS, plays a dominant role in dictating the miscibility and interaction landscape of these blend systems. In contrast to previous studies on PEO_{114}-*b*-$PCHC_{268}$ blends, the incorporation of POSS significantly alters the distribution of inter- and intramolecular free C=O and hydrogen-bonded C=O groups. Furthermore, the addition of Phenolic moieties effectively promotes the formation of robust intermolecular interactions, as evidenced in Figs. S3 and S4 [29].

3.3. Reaction induced self-assembled behavior of phenolic/PEO-b-PCHCPOSS binary blends

Fig. 6(a) shows the SAXS analyses of the phenolic/PEO-*b*-PCHCPOSS-2 blends containing different ratios of phenolic resin. Pure PEO-*b*-PCHCPOSS2 diblock copolymer exhibits no discernible SAXS peak, indicating that the system lacks long-range microphase separation, which is also consistent with DSC analysis based on single T_g value. The solubility parameter of PEO and PCHC is 9.4 and 10.2 $(cal/cm^3)^{1/2}$ [47], respectively, and thus the χN may not be high enough to form microphase separation. After adding phenolic resin could induce selective and compete hydrogen bonding within the PEO domain rather than PCHCPOSS domain, increasing ΔK and effective χ value, which generated clear compositional contrast that produces a primary SAXS peak. All blend systems exhibit a single, composition-dependent scattering peak, corresponding to a characteristic domain spacing ($d = 2\pi/q$), in the range of 30–44 nm. Because phenolic resin acts as both a hydrogen-bond donor and a diluent, it increases the effective volume fraction of the PEO rich phase, thereby expanding or swelling the domain spacing where the q^* value generally shifted toward lower q value. For example, the *d*-spacing of phenolic/PEO-*b*-PCHCPOSS-2 = 40/60 blend was 30.65 nm, which was increased to 43.63 nm for 70/30 blend. The absence of higher order scattering peaks, suggesting that the system does not form a well-ordered long-range periodic morphology and the microphase separation with short-range order because of the strong concentration fluctuations induced by hydrogen bonding. Fig. 6(c) also displays the SAXS profiles of the phenolic/PEO-*b*-PCHCPOSS-5 blends containing different phenolic resin ratios. The similarly trend was observed compared with phenolic/PEO-*b*-PCHCPOSS-2 blends where the pure PEO-*b*-PCHCPOSS-5 diblock copolymer exhibits no discernible SAXS peak and after adding phenolic resin, only the primary scattering peak was observed. The overall trend of q^* shifting to lower values with increasing phenolic content is observed in both 2 wt% and 5 wt% POSS blends because phenolic selectively partitions into the PEO-rich domains through strong hydrogen bonding, thereby enhancing compositional contrast. However, the *d*-spacing in the 5 wt% POSS system is smaller because the higher POSS loading significantly reduces the swelling capability of the PEO-rich domains. Phenolic molecules are partially diverted toward hydrogen bonding with the siloxane surfaces of POSS cages, leaving fewer phenolic species available to swell the PEO chains. Moreover, the rigid POSS nanocages impose packing constraints and local structural frustration, suppressing domain expansion. As a result, the domain spacing remains smaller than that in the 2 wt% POSS blends despite exhibiting the same compositional trend.

Fig. 6(b) and 6(d) display the SAXS profiles of the phenolic/PEO-*b*-PCHCPOSS-2 and phenolic/PEO-*b*-PCHCPOSS-5 blends after thermal curing at 150 °C. Compared with the uncured samples at 25 °C, all thermal curing blends exhibit a shift of the primary scattering maximum q toward higher q values, corresponding to a reduction of the domain spacing from ca. 30–44 nm before curing to ca. 25–38 nm for the 2 wt% POSS system and 20–26 nm for the 5 wt% POSS system. This indicates that the overall microdomain size contracts during phenolic curing. The decrease in *d*-spacing could be rationalized by the thermal curing chemistry of the phenolic resin. At lower temperatures, phenolic chains strongly hydrogen-bonded to the PEO/POSS-rich domains and act as a swelling agent, enlarging the characteristic length scale. Upon thermal curing at 150 °C, the structural evolution was observed due to the reaction-induced microphase separation (RIMPS) process. As a result, the thermal cured blends display much ordered microphase separation structure than the uncured samples, evidenced by the emergence of a single pronounced q^* peak ratios with $\sqrt{3}$ and even $\sqrt{4}$ shoulder at 30 and 40 wt% phenolic resin with PEO-*b*-PCHCPOSS-2 blends, suggesting that local hexagonal packing cylinder is achieved. For the 5 wt% POSS blends (Fig. 6(d)), the *d*-spacing is further reduced relative to the 2 wt% POSS analogues. The higher POSS loading introduces more rigid inorganic cages in the diblock copolymer, which restricts phenolic-induced swelling and imposes additional packing constraints, effectively "condensing" the microdomains. In addition, phenolic OH groups preferentially interact with the siloxane surfaces of POSS, further decreasing the amount of phenolic available to swell the PEO chains. As a result, after curing the 5 wt% POSS systems retain the same qualitative q^* trend with composition as the 2 wt% systems, but with systematically smaller domain spacing and a more confined morphology that is essentially frozen in by the crosslinked phenolic network. In Fig. S5, after thermal curing of the phenolic/PEO-*b*-PCHCPOSS-5 at 150 °C, the morphology observed by TEM is consistent with the SAXS analysis, exhibiting a cylindrical structure. However, because the template has not yet been removed, it may hinder the visualization of the mesoporous structure, rendering the pore features in the TEM images not clearly distinguishable.

3.4. Mesoporous phenolic resin templated by PEO-b-PCHCPOSS diblock copolymer

To obtain mesoporous phenolic resins templated by PEO-*b*-PCHCPOSS, the thermal analyses of pure PEO-*b*-PCHCPOSS diblock copolymers were determined by TGA analyses as displayed in Fig. 2(f), the much lower thermal decomposition temperature of diblock copolymers were found than pure PEO segment that are suitable as a template for mesoporous materials. Thermal calcination at 350 °C was used to remove PEO-*b*-PCHCPOSS diblock copolymer that is the same of PEO-*b*-PCL template to prepare mesoporous phenolic in this study as shown in Scheme S2 [17]. Fig. S6 displays the SAXS analyses of the phenolic/PEO-*b*-PCHCPOSS-2 = 40/60 blend before and after thermal treatment that removes the PEO-*b*-PCHCPOSS template. In Fig. S6(a), the primary scattering peak is observed at $q^* = 0.212\ nm^{-1}$, corresponding to the *d*-spacing of 29.64 nm. The absence of clear higher-order reflections suggests that the self-assembled structure lacks long-range order after thermal curing and is most consistent with disordered micellar order or wormlike structure. After thermal curing and template removal (Fig. S6(b)), the intensity of SAXS pattern increased significantly and became more ordered structure. A sharper primary peak was appeared at $q^* = 0.274\ nm^{-1}$, corresponding to the *d*-spacing of 22.91 nm. In addition, the peaks ratios of $\sqrt{3}$ and even $\sqrt{4}$ shoulder with a more regular hexagonal cylindrical structure. The thermal pyrolysis could reduce the domain size about 22.7% and such shrinkage is a typical for mesoporous phenolic resin after thermal condensation.

Fig. 7(a)-7(c) display SAXS analyses of the mesoporous phenolic materials templated from phenolic/PEO-*b*-PCHCPOSS-2 blends after thermal curing and pyrolysis at 350 °C. Fig. 7(a) exhibits the mesoporous phenolic material formed from phenolic/PEO-*b*-PCHCPOSS-2 = 30/70 blend, only a primary scattering maximum (q^*) at $0.235\ nm^{-1}$ with *d*-spacing of 26.74 nm, suggesting relatively loosely micellar or disordered cylinders, as confirmed by TEM image in Fig. 7(d). This feature indicates short-range ordering but no long-range periodic structure. The N_2 adsorption–desorption isotherm as shown in Fig. 7(g) shows a type-IV profile with an H3-type hysteresis loop, characteristic of disordered mesoporous frameworks with interconnected or slit-like pores.

This behavior is fully consistent with the SAXS result and TEM image with reveal disordered micellar-like pore arrangements without long-

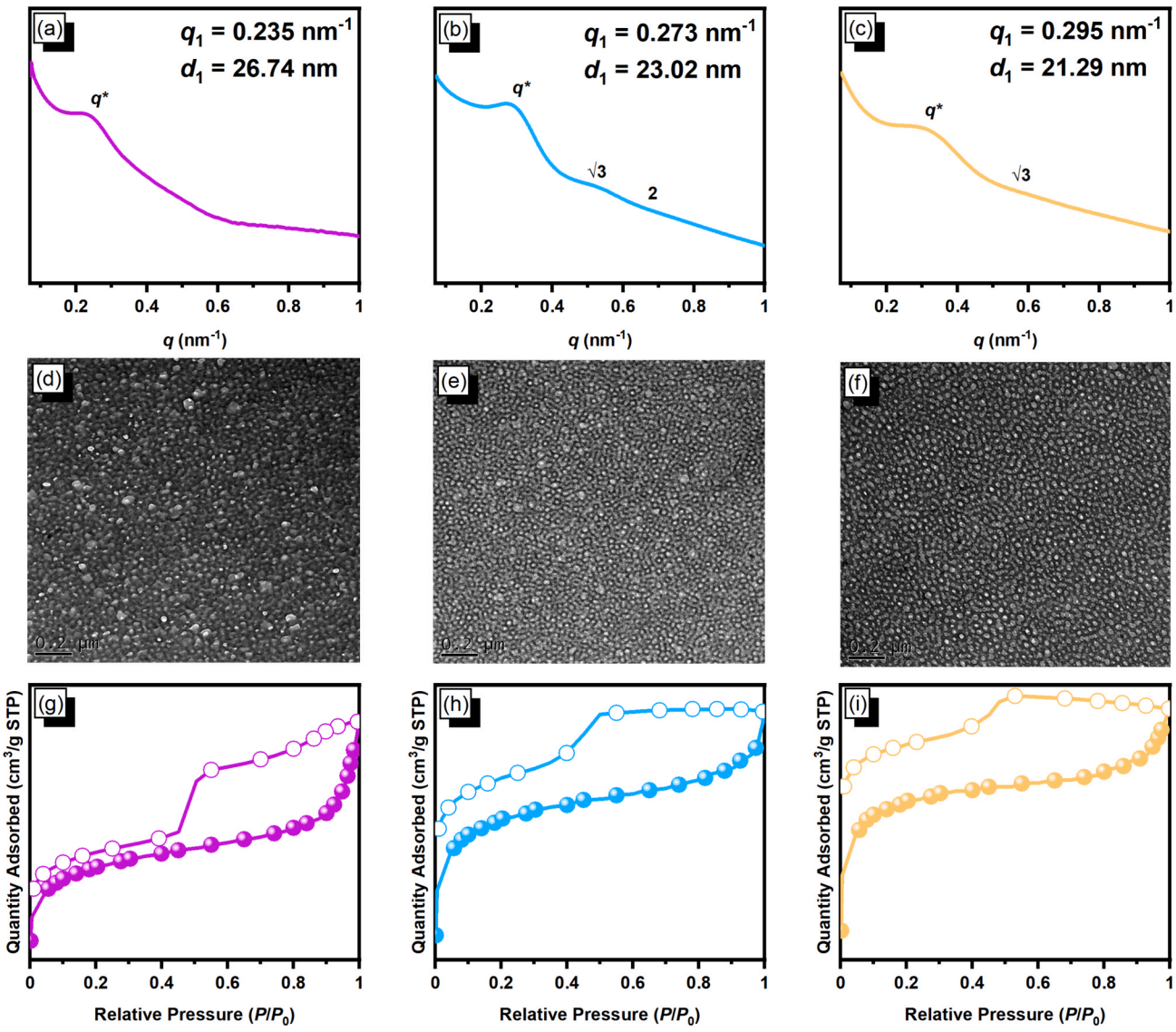

Fig. 7. SAXS profiles, TEM and N_2 adsorption–desorption isotherms of mesoporous phenolic materials derived from phenolic/PEO-*b*-PCHCPOSS-2 blends with compositions of (a, d, g) 30/70, (b, e, h) 40/60, and (c, f, i) 50/50 after thermal calcination at 350 °C.

range hexagonal order. Further increasing phenolic resin to 40 wt%, Fig. 7(b) displays SAXS pattern of mesoporous phenolic resin templated by phenolic/PEO-*b*-PCHCPOSS-2 = 40/60 blend, with the peak ratio of $1:\sqrt{3}:\sqrt{4}$ with more regular hexagonal cylindrical structure and already as mentioned in Fig. S6(b) (q^* = 0.274 nm^{-1}, *d*-spacing = 22.91 nm), as also confirmed by TEM image in Fig. 7(e). It reveals a denser array of nanoscale pores with relatively narrow size distribution and homogeneous spatial arrangement. The N_2 adsorption–desorption isotherm as shown in Fig. 7(h) shows a type-IV profile with an H3-type hysteresis loop, characteristic of slit-shaped or wormlike inter-particle mesopores. An extended uptake at high relative pressures (P/P_0 = 0.7–1.0) indicates an interconnected mesopore network rather than isolated spherical pores. The SAXS pattern of mesoporous phenolic resin templated by phenolic/PEO-*b*-PCHCPOSS-2 = 50/50 blend shows the primary peak (q^*) at 0.295 nm^{-1} with *d*-spacing of 21.29 nm. A weak but visible secondary feature at $q/q^* = \sqrt{3}$ indicates the short-range hexagonal-like correlations. Fig. 7(f) reveals the TEM image with a densely packed nanostructure consisting of uniform, closely spaced mesopores with narrow size distribution, matching the SAXS analyses. N_2 adsorption–desorption measurements exhibit a Type-IV isotherm with a strong H3 hysteresis loop as shown in Fig. 7(i), consistent with an accessible network of interconnected wormlike or slit-shaped mesopores.

Fig. 8(a)-8(c) show SAXS patterns of mesoporous phenolic resin templated from phenolic/PEO-*b*-PCHCPOSS-5 blends after thermal curing and pyrolysis at 350 °C. Fig. 8(a) displays the mesoporous phenolic resin templated by phenolic/PEO-*b*-PCHCPOSS-5 = 30/70 blend where the primary scattering peak at q^* = 0.215 nm^{-1} with *d*-spacing = 29.22 nm. The presence of a weak secondary feature at $q/q^* = \sqrt{3}$ suggests the short-range hexagonal-like structure. However, the higher-order reflections are notably weaker and less well resolved than those in the 2 wt% POSS samples, indicating reduced long-range structural coherence. This behavior implies that increasing the POSS content to 5 wt% does not significantly alter the average pore–pore spacing, but instead disrupts the regular packing of the templated domains. The higher concentration of rigid silsesquioxane cages increases local packing frustration and suppresses the development of long-range periodic order, leading to a mesostructure dominated by short-range correlations, as confirmed by TEM image as shown in Fig. 8(d). The wormlike and locally distorted mesoporous domains suggests that increased POSS loading introduces packing frustration and suppresses long-range ordering while preserving the characteristic mesoscale length. The N_2 adsorption–desorption isotherm of the mesoporous

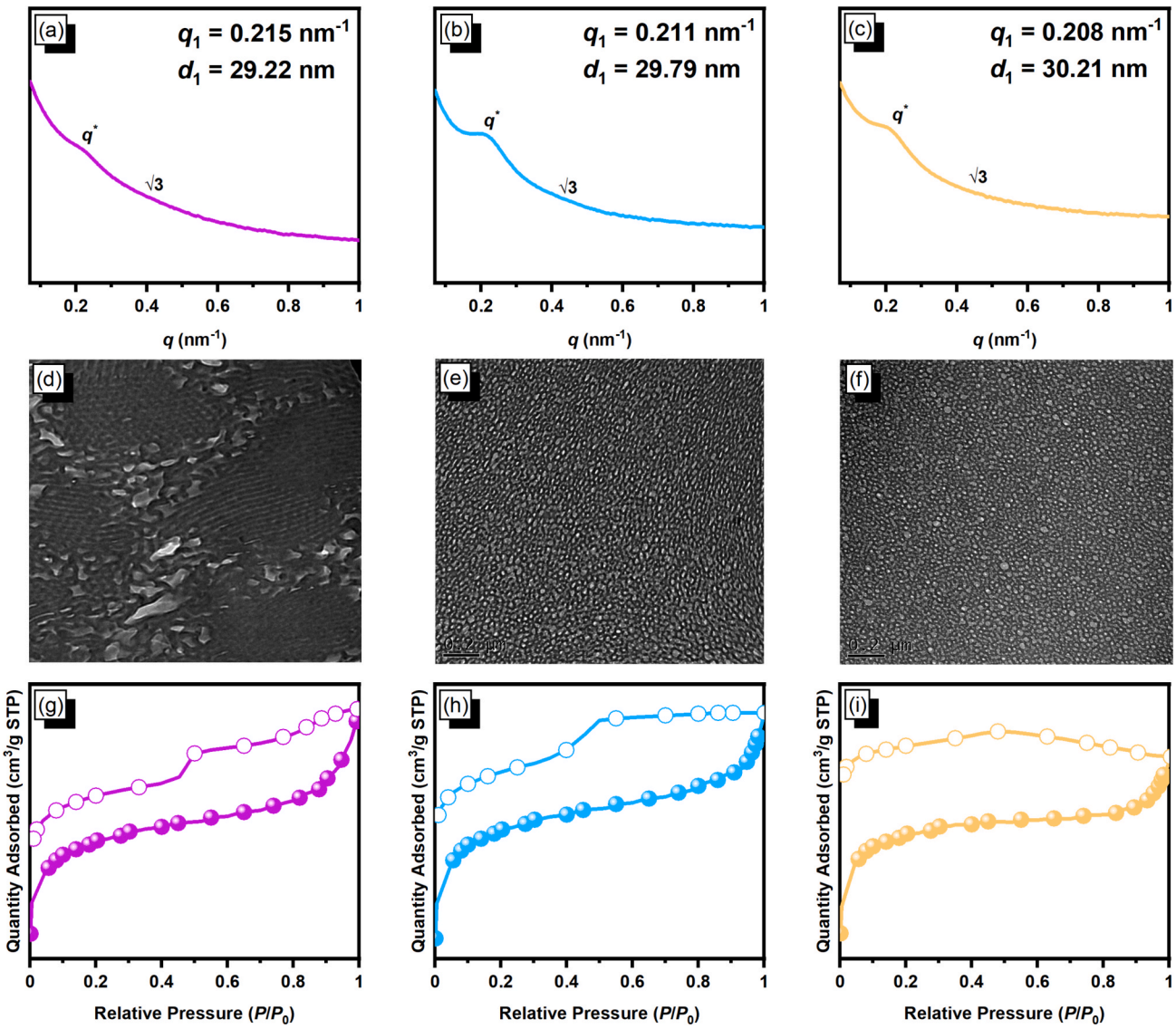

Fig. 8. SAXS profiles, TEM and N_2 adsorption–desorption isotherms of mesoporous phenolic materials derived from phenolic/PEO-*b*-PCHCPOSS-5 blends with compositions of (a, d, g) 30/70, (b, e, h) 40/60, and (c, f, i) 50/50 after thermal calcination at 350 °C.

phenolic resin templated by the 5 wt% POSS-containing diblock copolymer (Fig. 8(g)) also exhibits a Type IV profile, characteristic of mesoporous materials. A pronounced H3-type hysteresis loop is observed over the intermediate-to-high relative pressure range ($P/P_0 \approx 0.4$–1.0), indicating the presence of interconnected, non-cylindrical mesopores, such as slit-like or wormlike pore geometries.

Further increasing phenolic resin to 40 wt%, Fig. 8(b) displays SAXS pattern of mesoporous phenolic resin templated by phenolic/PEO-*b*-PCHCPOSS-5 = 40/60 blend, with the peak ratio of 1:$\sqrt{3}$ with short-range hexagonal cylindrical structure (q^* = 0.211 nm^{-1}, *d*-spacing = 29.79 nm), as also confirmed by TEM image in Fig. 8(e). A highly homogeneous mesoporous morphology composed of densely packed nanoscale pores with a relatively narrow size distribution. Although no long-range periodic lattice is observed, the pores exhibit clear short-range positional correlations, forming locally ordered domains with uniform spacing. The corresponding N_2 adsorption–desorption isotherm (Fig. 8(h)) displays a type IV profile, characteristic of mesoporous materials, together with a pronounced H3-type hysteresis loop over the relative pressure range of $P/P_0 \approx 0.4$–1.0. This hysteresis behavior indicates the presence of interconnected mesopores with slit-like or wormlike geometries, rather than isolated cylindrical pores. The SAXS pattern of mesoporous phenolic resin templated by phenolic/PEO-*b*-PCHCPOSS-5 = 50/50 blend shows the primary peak (q^*) at 0.208 nm^{-1} with *d*-spacing of 30.21 nm. The shift of the primary peak toward lower *q* values indicates an increased pore–pore center distance, consistent with a higher effective volume fraction of the block-copolymer template and reduced framework contraction. Only a weak but visible secondary feature at $q/q^* = \sqrt{3}$ is discernible, and higher order reflections are absent, suggesting microphase separation occurring, the limited short-range order. The uniformly dispersed yet weakly interacting mesopores is confirmed by TEM image (Fig. 8(f)) and a Type IV N_2 sorption isotherm with a subdued hysteresis loop, indicating reduced pore connectivity (Fig. 8(i). The BET surface area, pore size and pore volume of the mesoporous phenolic resins are summarized in Table 2.

In general, the total BET surface area and the pore volume were decreased upon increasing phenolic concentrations of the templated PEO-*b*-PCHCPOSS diblock copolymers. To the best of our knowledge, this study is the first to fabricate mesoporous phenolic resin using POSS-based diblock copolymer. Because the POSS units are covalently grafted to the PCHC backbone, they are confined to the PCHC-rich domains during RIPS. Upon pyrolysis, PCHC is removed to form mesopores, while the phenolic carbon matrix shrinks and rigidifies, forcing the thermally

Table 2
Textual properties of the mesoporous phenolic materilas templated from PEO-*b*-PCHCPOSS-2 and PEO-*b*-PCHCPOSS-5.

Phenolic/ PEO-*b*-PCHCPOSS-2	*d*-spacing (nm)	S_{BET} (m^2/g)	Pore size (nm)	Pore volume (cm^3/g)
30/70	26.74	536.9	11.36	0.146
40/60	23.02	427.7	11.04	0.144
50/50	21.29	310.9	11.32	0.111
Phenolic/ PEO-*b*-PCHCPOSS-5				
30/70	29.22	419.3	10.76	0.112
40/60	29.72	375.2	10.81	0.108
50/50	30.21	171.2	12.65	0.056

stable POSS residues to remain anchored at the pore walls rather than migrating into the pore center. This wall-selective retention of POSS is thermodynamically favored due to the strong interfacial affinity of the Si–O cage toward the phenolic surface, consistent with the SEM EDS mapping results as shown in Fig. 9, which reveals a heterogeneous surface morphology featuring nanoscale domains uniformly embedded within the polymer matrix, indicating good dispersion without obvious macroscopic phase separation or aggregation (Fig. 9(b)), corresponding EDS spectra confirm the elemental composition of the composite, showing dominant signals from C (Fig. 9(c)) and O (Fig. 9(d)), consistent with the organic polymer backbone. A distinct Si signal is also observed, verifying the successful incorporation of POSS cages into the polymer matrix (Fig. 9(e)).

4. Conclusions

In summary, POSS-containing CO_2-derived diblock copolymer templates were successfully developed to generate thermally robust mesoporous phenolic resin. Blending with phenolic resin produced microphase separation, as evidenced by two composition-dependent T_g behavior and FTIR analysis revealed competitive hydrogen bonding among phenolic OH groups, PEO ether units, PCHC carbonate groups, and POSS siloxane cages. SAXS further showed that phenolic addition induces the microphase separation in otherwise weakly segregated PEO-*b*-PCHCPOSS diblock copolymer, and that thermal curing at 150 °C promotes reaction-induced microphase separation to lock in locally ordered self-assembled nanostructures. Subsequent pyrolysis at 350 °C removed the PEO-*b*-PCHCPOSS diblock copolymer template and yielded mesoporous phenolic frameworks with tunable pore as also confirmed by TEM image and BET analyses. The POSS moieties covalently anchored to the PCHC segments are preferentially retained at the pore walls after template removal, leading to inorganic cage-enriched pore surfaces that enhance structural stability and inhibit pore collapse during thermal processing. Increasing the POSS loading from 2 to 5 wt% largely preserved the mesoscale spacing but diminished structural coherence, consistent with packing frustration introduced by the rigid cages and partial diversion of phenolic hydrogen bonding toward POSS surfaces, which limits phenolic-driven swelling and suppresses the development of more ordered pore correlations. Overall, this work establishes a CO_2-derived diblock copolymer/POSS hybrid templating platform in which the mesoscale structure and porosity of phenolic frameworks could be systematically tuned through controlled hydrogen-bonding competition, POSS content, and thermal processing.

CRediT authorship contribution statement

Yen-Min Lo: Writing – original draft, Formal analysis, Data curation. **Yen-Ling Kuan:** Writing – original draft, Data curation, Conceptualization. **Yang-Chin Kao:** Formal analysis, Data curation. **Junko Aimi:** Resources, Formal analysis. **Chih-Feng Huang:** Supervision, Resources, Funding acquisition. **U-Ser Jeng:** Resources, Formal analysis, Data curation. **Shiao-Wei Kuo:** Writing – review & editing, Supervision, Formal analysis, Conceptualization.

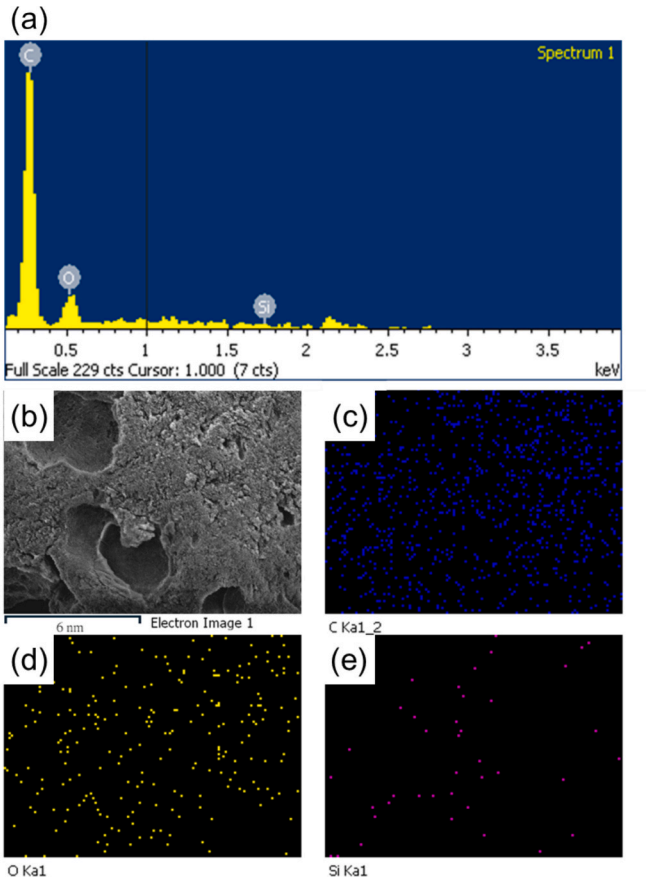

Fig. 9. (a) SEM-EDS analyses, (b) SEM image, (c) C, (d) O, and (e) Si-mapping of mesoporous phenolic material derived from phenolic/PEO-*b*-PCHCPOSS-5 = 50/50 blend.

Declaration of competing interest

The authors declare that they have no known competing financial interests or personal relationships that could have appeared to influence the work reported in this paper.

Acknowledgments

This study was supported financially by the National Science and Technology Council, Taiwan, under contracts NSTC 114-2223-E-110-001- and 113-2221-E-110-012-MY3. The authors thank the staff at National Sun Yat-sen University, Taiwan for their assistance with the TEM (ID: EM022600) experiments.

Appendix A. Supplementary data

Supplementary data to this article can be found online at https://doi.org/10.1016/j.eurpolymj.2026.114848.

Data availability

The data that has been used is confidential.

References

[1] X. Yang, L. Zhang, F. Zhang, Y. Huang, Y. Chen, Sulfur-infiltrated graphene-based layered porous carbon cathodes for high-performance lithium–sulfur batteries, ACS Nano 8 (2014) 5208–5215, https://doi.org/10.1021/nn501284q.

[2] R. Liu, L. Wan, S. Liu, L. Pan, D. Wu, D. Zhao, An interface-induced co-assembly approach towards ordered mesoporous carbon/graphene aerogel for high-performance supercapacitors, Adv. Funct. Mater. 25 (2015) 526–533, https://doi.org/10.1002/adfm.201403280.
[3] P. Veerakumar, N. Dhenadhayalan, K.C. Lin, S.B. Liu, Highly stable ruthenium nanoparticles on 3D mesoporous carbon: an excellent opportunity for reduction reactions, J. Mater. Chem. A 3 (2015) 23448–23457, https://doi.org/10.1039/C5TA06875D.
[4] Z.-L. Yu, Y.-C. Gao, B. Qin, Z.-Y. Ma, S.-H. Yu, Revitalizing traditional phenolic resin toward a versatile platform for advanced materials, Acc. Mater. Res. 5 (2024) 146–159, https://doi.org/10.1021/accountsmr.3c00194.
[5] Y. Miyamori, Y. Kong, Y. Nabae, K. Hatakeyama-Sato, T. Hayakawa, Highly ordered bimodal mesoporous carbon from ABC triblock terpolymers with phenolic resol, ACS Macro Lett. 13 (2024) 1698–1703, https://doi.org/10.1021/acsmacrolett.4c00651.
[6] R. Otero, D. Esquivel, M.A. Ulibarri, F.J. Romero-Salguero, P. Van Der Voort, J. M. Fernández, Mesoporous phenolic resin and mesoporous carbon for the removal of S-metolachlor and bentazon herbicides, Chem. Eng. J. 251 (2014) 92–101, https://doi.org/10.1016/j.cej.2014.04.038.
[7] Q. Tian, X.-K. Zeng, C. Zhao, L.-Y. Jing, X.-W. Zhang, J. Liu, Exceptional photocatalytic hydrogen peroxide production from sandwich-structured graphene interlayered phenolic resin nanosheets with mesoporous channels, Adv. Funct. Mater. 33 (2023) 2213173, https://doi.org/10.1002/adfm.202213173.
[8] A.K. Mishra, J. Lee, S. Kang, E. Kim, C. Choi, J.K. Kim, Gallol-based block copolymer with a high Flory–Huggins interaction parameter for next-generation lithography, Macromolecules 55 (2022) 10797–10803, https://doi.org/10.1021/acs.macromol.2c01633.
[9] Y.C. Kao, K.T. Yeh, M.G. Mohamed, H. Karim, W.H. Su, S.W. Kuo, Structural modulation via mesoporous silica templating in covalent organic frameworks: Converting functional aspects for adsorption behavior, Sep. Purfi. Technol. 375 (2025) 133827, https://doi.org/10.1016/j.seppur.2025.133827.
[10] T. Chou, W. Chen, M.G. Mohamed, Y. Huang, S.W. Kuo, Organic–inorganic phenolic/POSS hybrids providing highly ordered mesoporous structures templated by PS-b-P4VP diblock copolymer, Chem Eur J 29 (2023) e202300538, https://doi.org/10.1002/chem.202300538.
[11] J.G. Li, W.C. Chu, U.S. Jeng, S.W. Kuo, In situ monitoring of reaction-induced self-assembly of phenolic resin templated by diblock copolymers, Macromol. Chem. Phys. 214 (2013) 2115–2123, https://doi.org/10.1002/macp.201300332.
[12] A. Zenati, A. Pokhrel, Properties and molecular self-assembly of liquid crystalline diblock and triblock copolymers influenced by Flory–Huggins interaction parameter, J. Polym. Sci. 61 (2023) 1596–1611, https://doi.org/10.1002/pol.20230075.
[13] Z. Xu, S. Zheng, Reaction-induced microphase separation in epoxy thermosets containing poly(ε-caprolactone)-block-poly(n-butyl acrylate) diblock copolymer, Macromolecules 40 (2007) 2548, https://doi.org/10.1021/ma062486v.
[14] R. Yu, S. Zheng, X. Li, J. Wang, Reaction-induced microphase separation in epoxy thermosets containing block copolymers of polystyrene and poly(ε-caprolactone), Macromolecules 45 (2012) 9155–9168, https://doi.org/10.1021/ma3017212.
[15] C.-F. Huang, W.-H. Chen, J. Aimi, Y.-S. Huang, S. Venkatesan, Y.-W. Chiang, S.-H. Huang, S.-W. Kuo, T. Chen, Synthesis of well-defined PCL-b-PnBA-b-PMMA ABC triblock copolymers toward nanostructures in epoxy thermosets, Polym. Chem. 9 (2018) 5644–5654, https://doi.org/10.1039/C8PY01357H.
[16] C.W. Chiou, Y.C. Lin, L. Wang, R. Maeda, T. Hayakawa, S.W. Kuo, Hydrogen-bond interactions mediate hierarchical self-assembly of POSS-containing block copolymers blended with phenolic resin, Macromolecules 47 (2014) 8709–8721, https://doi.org/10.1021/ma502180c.
[17] T.C. Chou, S.W. Kuo, Controllable wet-brush blending of linear diblock copolymers with phenolic/DDSQ hybrids toward mesoporous structure phase diagram, Macromolecules 57 (2024) 5958–5970, https://doi.org/10.1021/acs.macromol.4c00665.
[18] A.C. Balazs, Modeling self-assembly and phase behavior in complex mixtures, Annu. Rev. Phys. Chem. 58 (2007) 211–233, https://doi.org/10.1146/annurev.physchem.58.032806.104520.
[19] J.G. Li, Y.D. Lin, S.W. Kuo, From microphase separation to self-organized mesoporous phenolic resin through competitive hydrogen bonding with double-crystalline diblock copolymers, Macromolecules 44 (2011) 9295–9309, https://doi.org/10.1021/ma2010734.
[20] J. Wei, Z. Sun, W. Luo, Y. Li, A.A. Elzatahry, A.M. Al-Enizi, Y. Deng, D. Zhao, New insight into the synthesis of large-pore ordered mesoporous materials, J. Am. Chem. Soc. 139 (2017) 1706–1713, https://doi.org/10.1021/jacs.6b11411.
[21] Y. Deng, C. Liu, D. Gu, T. Yu, B. Tu, D. Zhao, Thick wall mesoporous carbons with large pore structure templated from weakly hydrophobic PEO-PMMA diblock copolymer, J. Mater. Chem. 18 (2008) 91–97, https://doi.org/10.1039/B713310C.
[22] J.G. Li, P.Y. Lee, M.M. Ahmed, M.G. Mohamed, S.W. Kuo, Varying hydrogen bonding strength in phenolic/PEO-b-PLA blends provides mesoporous carbons with large accessible pores for energy storage, Macromol. Chem. Phys. 221 (2020) 2000040, https://doi.org/10.1002/macp.202000040.
[23] Y. Qin, X. Sheng, S. Liu, G. Ren, X. Wang, F. Wang, Recent advances in carbon dioxide based copolymers, J. CO2 Util. 11 (2015) 3–9, https://doi.org/10.1016/j.jcou.2014.10.003.
[24] P.E. Jacky, A.D. Easley, B.P. Fors, Controlled anionic polymerization mediated by carbon dioxide, Nat. Chem. 17 (2025) 1076–1082, https://doi.org/10.1038/s41557-025-01819-7.
[25] Y. Ma, Z. Wang, L. Jiang, J. Zhang, C. Ren, X. Kou, S. Liu, Z. Li, Bulky phosphazenium salt controlling chemoselective terpolymerization of epoxide, anhydride and CO2, Angew. Chem. Int. Ed. 64 (2024) e202416104, https://doi.org/10.1002/anie.202416104.
[26] Y. Wang, Y. Zhao, Y. Ye, H. Peng, X. Zhou, X. Xie, X. Wang, F. Wang, One-step route to CO2-based block copolymers by simultaneous ROCOP of CO2/epoxides and RAFT polymerization, Angew. Chem. Int. Ed. 57 (2018) 3593–3597, https://doi.org/10.1002/anie.201710734.
[27] G.-W. Yang, R. Xie, Y.-Y. Zhang, C.-K. Xu, G.-P. Wu, Evolution of copolymers of epoxides and CO2: catalysts, monomers, architectures and applications, Chem. Rev. 124 (2024) 12305, https://doi.org/10.1021/acs.chemrev.4c00517.
[28] F. Butler, F. Fiorentini, K.H.S. Eisenhardt, C.K. Williams, Heterodinuclear Co(III)Na (I) catalysts for ROCOP of propene oxide and CO2, Macromolecules 58 (2025) 7150–7160, https://doi.org/10.1021/acs.macromol.5c01529.
[29] W.T. Du, S.Y. Chen, S.W. Kuo, Mesoporous phenolic/carbon materials templated by CO2-based PEO-b-PCHC diblock copolymers for CO2 capture, J. CO2 Util. 80 (2024) 102702, https://doi.org/10.1016/j.jcou.2024.102702.
[30] Y.-J. Lee, S.-W. Kuo, W.-J. Huang, H.-Y. Lee, F.-C. Chang, Miscibility, specific interactions and self-assembly behavior of phenolic/POSS hybrids, J. Polym. Sci. B Polym. Phys. 42 (2004) 1127, https://doi.org/10.1002/polb.10762.
[31] S.-W. Kuo, F.-C. Chang, POSS related polymer nanocomposites, Prog. Polym. Sci. 36 (2011) 1649–1696, https://doi.org/10.1016/j.progpolymsci.2011.05.002.
[32] S.-W. Kuo, Hydrogen bonding interactions in polymer/POSS nanomaterials, J. Polym. Res. 29 (2022) 69, https://doi.org/10.1007/s10965-021-02885-4.
[33] D. Wang, J. Ding, B. Wang, Y. Zhuang, Z. Huang, Synthesis and thermal degradation of POSS-modified phenolic resin, Polymers 13 (2021) 1182, https://doi.org/10.3390/polym13081182.
[34] M.R.S. Silveira, C.A. Ferreria, L. Ferry, J.M. Lopez-Cuesta, Flame retardancy of phosphorus-containing novolac epoxy-silsesquioxanes, Thermochim Acta 753 (2025) 180139, https://doi.org/10.1016/j.tca.2025.180139.
[35] T. Nishimura, C.J. Cheng, Y. Oishi, T.W. Chang, F. Li, T. Gao, R. Borsali, T. Yamamoto, K. Tajima, H.L. Chen, T. Satoh, I. Isono, Molecular design of POSS–oligosaccharide hybrid materials for stabilizing soft-matter quasicrystals, Macromolecules 59 (2026) 231–241, https://doi.org/10.1021/acs.macromol.5c02976.
[36] H. Wang, G. Hang, B. Zhao, T. Zhang, L. Li, S. Zheng, Poly(cyclooctadiene-co-ionic liquid) networks cross-linked via POSS–POSS interactions, Macromolecules 58 (2025) 3816–3831, https://doi.org/10.1021/acs.macromol.4c02783.
[37] G. Li, D. Jiang, P. Ren, H. Zhao, K. Zhang, L. Chang, Z. Liu, S. Pu, "Clicking" amphiphilic block copolymers onto POSS core: a general approach for star-like polymers, Giant 21 (2025) 100346, https://doi.org/10.1016/j.giant.2024.100346.
[38] T. Hirai, M. Leolukman, S. Jin, R. Goseki, Y. Ishida, M.-A. Kakimoto, T. Hayakawa, M. Ree, P. Gopalan, Hierarchical self-assembled structures from POSS-containing block copolymers, Macromolecules 42 (2009) 8835–8843, https://doi.org/10.1021/ma9018944.
[39] W.T. Du, Y.L. Kuan, S.W. Kuo, Intra- and intermolecular hydrogen bonding in blends of CO2/epoxy cyclohexene copolymer with poly(vinyl phenol), Int. J. Mol. Sci. 23 (2022) 7018, https://doi.org/10.3390/ijms23137018.
[40] Y.L. Kuan, W.T. Du, S.W. Kuo, Effect of POSS nanoparticles on miscibility and hydrogen bonding behavior of CO2-based poly(cyclohexene carbonate) copolymers, J. Taiwan Inst. Chem. Eng. 153 (2023) 105214, https://doi.org/10.1016/j.jtice.2023.105214.
[41] Y.L. Kuan, Y.C. Chiu, Y.S. Ye, S.W. Kuo, Design of CO2-derived poly(cyclohexene carbonate) copolymers to mediate intra-/intermolecular interactions, Macromolecules 58 (2025) 1090–1102, https://doi.org/10.1021/acs.macromol.4c02295.
[42] M.J. Yu, Y.L. Kuan, W.T. Du, S.W. Kuo, Effect of side chain length on miscibility and hydrogen bonding interactions of CO2-based copolymers, Polymer 344 (2026) 129550, https://doi.org/10.1016/j.polymer.2025.129550.
[43] Y.L. Kuan, C.W. Chu, W.T. Du, S.W. Kuo, Macromolecules 59 (2026) 1346–1357, https://doi.org/10.1021/acs.macromol.5c03069.
[44] A. Thevenon, J.A. Garden, A.J.P. White, C.K. Williams, Dinuclear zinc salen catalysts for ROCOP of epoxides and carbon dioxide, Inorg. Chem. 54 (2015) 11906–11915, https://doi.org/10.1021/acs.inorgchem.5b02233.
[45] Y.-Y. Zhang, G.-W. Yang, Y. Wang, X.-Y. Lu, G.-P. Wu, Z.-S. Zhang, K. Wang, R.-Y. Zhang, P.F. Nealey, D.J. Darensbourg, et al., Synthesis of CO2-based block copolymers via chain transfer polymerization using macroinitiators, Macromolecules 51 (2018) 791–800, https://doi.org/10.1021/acs.macromol.7b02231.
[46] S.-W. Kuo, Hydrogen Bonding in Polymeric Materials. Wiley-VCH (2018), https://doi.org/10.1002/9783527804276.
[47] M.M. Coleman, J.F. Graf, P.C. Painter, Specific Interactions and the Miscibility of Polymer Blends, Technomic, Lancaster, PA, 1991.